

# INVESTIGATING REACTOR COMPONENTS WITH THE COARSE-GRID-METHODOLOGY

**M. Viellieber and A. Class**

Institute for Nuclear and Energy Technologies (IKET)  
Hermann-von-Helmholtz-Platz 1  
76344 Eggenstein-Leopoldshafen  
Germany  
Mathias.Viellieber@kit.edu; Andreas.Class@kit.edu

## ABSTRACT

The core of a nuclear reactor is a few meters in height and diameter. It is composed of up to 800 hundred fuel assemblies which are again composed of tenth of fuel rods with a diameter of about 10 mm. Therefore the relevant length scales for CFD simulations range from the sub millimeter range, relevant for the fuel rod space up to several meters. Describing such a multi scale situation with Computational Fluid Dynamics (CFD) is challenging and the historical approach was to use integral descriptions, the so called sub channel analyses codes, that are closed by empirical and experimental correlations. A CFD simulation of a complete nuclear reactor set up resolving all relevant scales requires exceedingly large computational resources. However, in many cases there are repetitive geometrical assemblies and flow patterns allowing the general approach of creating a parametrized model for one segment and composing many of these reduced models to obtain the entire reactor simulation. With our method, the Coarse-Grid-CFD (CGCFD), we intend to replace the experimental or empirical input with CFD data. In an application the methodology starts with a detailed and well-resolved CFD simulation of one representative segment. From this simulation we extract in tabular form so-called volumetric forces which upon parametrization is assigned to all coarse cells. Repeating the fine simulation for multiple flow conditions parametrized data can be obtained to the desired degree of accuracy. Note, that parametrized data is used to close an otherwise strongly under resolved, coarsely meshed model of a complete reactor setup. Within this work we present the results of several fuel assemblies that were investigated with our methodology. Furthermore we show Coarse-Grid-CFD results of a 127 pin LBE cooled wire wrapped fuel assembly. General guidelines for the proper application of CGCFD, limits of its application and potential numerical cost saving are discussed.

## KEYWORDS

CGCFD, RANS, CFD, FUEL ASSEMBLY

## 1. INTRODUCTION

State of the art Computational Fluid Dynamic (CFD) tools allow engineers and scientists to investigate and predict fluid flows qualitatively and quantitatively. Among other research fields CFD simulations are widely used in nuclear applications for the layout and examination of safety relevant components in different flow regimes of the power plants. CFD-tools complement and sometimes replace expensive experimental investigations of components of power plants. In contrast to fluid experiments, CFD can predict full scale behavior of the real thermal hydraulics. The drawback of CFD simulations is the challenge that complex geometries and flow regimes or physic often need exhaustive computational resources, clock time and cost to obtain reliable results. For example a CFD simulation of a complete reactor core with all its built in

components including fuel rods, spacer grids, pin fixers etc. is not feasible with state of the art industrial CFD-Methods.

Within this paper the Coarse-Grid method is presented. The method represents a multi-scale approach that enables the simulation of geometries, which are computationally too extensive for state of the art CFD codes. The main features of the methodology are described within [11], where a detailed description of the methodology as well as the application of the methodology to a section of a water cooled rod bundle is shown. Within [2] the Anisotropic Porosity Formulation is introduced within the CGCFD Methodology. Within [12] the CGCFD methodology is applied to a seven pin wire wrapped water cooled fuel assembly and the hydraulic behavior of the CGCFD simulation is compared to RANS results. This paper gives an overview of the CGCFD methodology and shows validation results of a subchannel that is investigated by the CGCFD. The paper also describes the application of the method to a simulation of a Lead Bismuth Eutectic (LBE) cooled 19 and a 127 pin fuel rod bundle.

## 2. THEORY OF THE COARSE-GRID-METHOD

### 2.1. Methodology of a CGCFD simulation

Figure 2.1 illustrates the methodology of a CGCFD simulation for the case of a fuel rod bundle. A corresponding experiment is conducted within the KARlsruhe Liquid Metal LABORatory (KALLA) and details about the experiment and the CGCFD simulation of this rod bundle can be found in [1] and [2]. The most important precondition for CGCFD is, that the target of investigation has a repetitive geometrical and flow character e.g. a fuel assembly that consist of plenty of subchannels with almost the same geometry. In summary the following requirements are needed to conduct a CGCFD:

- The target of investigation consists of repeating flow structures.
- The physics of the target of investigation can be described with state of the art CFD.
- The entire target of investigation can't be simulated with state of the art CFD at reasonable cost and resources.

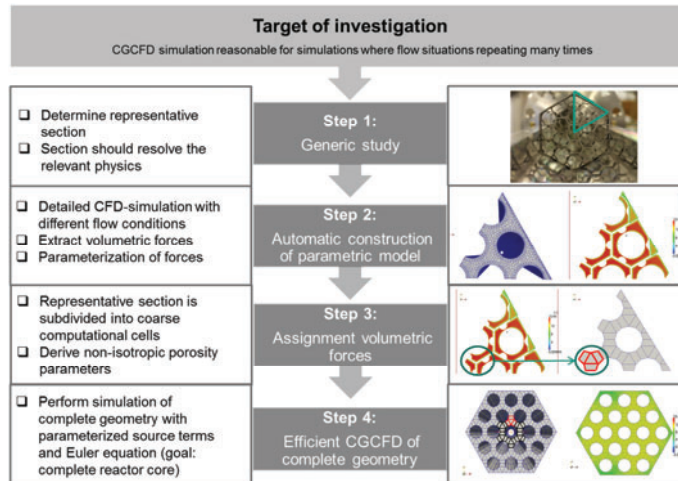


**Figure 2.1. CGCFD methodology.**

Figure 2-1 shows the schematically CGCFD methodology. The first step is to identify a single or a very small number of representative sections within the complete geometry under investigation. These representative sections should resolve the main physical processes of the complete domain. The selection of the representative section affects the results of the CGCFD simulation, as extracted integral data enter CGCFD simulations.

In the second step the representative section/sections are simulated employing state of the art CFD. This can either be Reynolds-Averaged-Navier-Stokes-Simulations (RANS) or Large Eddy Simulations (LES) and may even be Direct Numerical Simulations (DNS). Here best practice guidelines have to be followed (choice of turbulence model, mesh resolution, etc.), since results directly enter the CGCFD.

In step three the representative section is subdivided into coarse computational cells. The resolution of this mesh is chosen such that, in case of the here investigated fuel bundle, subchannel cross sections are resolved by a few coarse cells. Integral fluxes on surfaces and volume integrals of the coarse cells are computed and represent under-resolved physical information on the coarse mesh. This also includes non-resolved geometrical details resulting in non-isotropic porosity parameters. Step three is performed for multiple flow situations to allow parameterization. Well-known models of subchannel analysis codes help to determine an appropriate ansatz. Only a few representative simulations need to be performed.

In step four the complete target geometry is meshed with coarse cells, where each cell is identified with a corresponding cell in the representative section, so that the parametrized volumetric source terms and anisotropy porosity parameters can be provided for the final CGCFD of the target geometry.

The described methodology represents a multi-scale approach enabling computationally effective simulation of large geometries including a complete reactor core. CGCFD simulations are useful for geometries with repetitive flow characteristics and geometries where state of the art computational methods are too expensive. For these cases the methodology offers a systematic and automatically applicable tool for fast studies of large systems.

## 2.2. Mathematical formulation of the CGCFD

### Derivation of the volumetric source term

System codes are formulated for macroscopic control volumes where physical effects like friction losses and transport between neighboring channels are integrally described. For CGCFD, the required terms can be evaluated directly from fully resolved fields of a detailed CFD simulation. Equation (2.1) shows the momentum equation in conservative form for Reynolds Averaged Navier Stokes (RANS) simulations in the simplest form. The Reynolds averaged quantities in eq. (2.2.1),  $u$ ,  $p$ ,  $\rho$  and  $\mu$  are the fluid velocity, pressure, density, and the effective viscosity, respectively, and  $i, j = 1, 2, 3$ . The governing equation for the CGCFD is the Euler equation (2.2.2).

$$\rho [\partial_t u_i + \partial_{x_j} (u_i u_j)] + \partial_{x_i} p = \partial_{x_i} [\mu (\partial_{x_j} u_i + \partial_{x_i} u_j)], \quad (2.2.1)$$

$$\rho [\partial_t U_i + \partial_{x_j} (U_i U_j)] + \partial_{x_i} P = \vec{R}_J. \quad (2.2.2)$$

The capital  $U$  and  $P$  within Euler eq. (2.2.2) represent the CGCFD quantities and  $J$  is the control volume index. The Euler equation is extended by a volumetric source term  $\vec{R}_J$  that represents the non-resolved physical information. Without this source term equation (2.2.2) is not able to resolve the viscous physics like the viscous dissipation or turbulence effects. To derive  $\vec{R}_J$  and the later described porosity parameters, volume- and surface averages for arbitrary functions  $f$  across control volume  $\Omega_J$  and surfaces  $\Omega_{Jm}$  are introduced.

$$\langle f \rangle_{\Omega_J} = \frac{1}{\Omega_J} \iiint_{\Omega_J} f \, dV, \quad (2.2.3)$$

$$\langle f \rangle_{\Omega_{Jm}} = \frac{1}{\Omega_{Jm}} \iint_{\Omega_{Jm}} f \, dA. \quad (2.2.4)$$

A term by term balance is then applied between equation (2.2.1) and (2.2.2) for each control volume, which is yielding:

$$\langle u_i \rangle_{\Omega_J} = \langle U_i \rangle_{\Omega_J}, \quad (2.2.5)$$

$$\langle \partial_{x_i} p \rangle_{\Omega_J} = \langle \partial_{x_i} P \rangle_{\Omega_J}, \quad (2.2.6)$$

$$\langle \partial_{xj}(u_i u_j) \rangle_{\Omega_J} = \langle \partial_{xj}(U_i U_j) \rangle_{\Omega_J}. \quad (2.2.7)$$

Subtracting eq. (2.2.1) from eq. (2.2.2) leads to a conditional equation for the volumetric source term  $\vec{R}_J$  that reads discretized for a single control volume.

$$\langle \vec{R}_J \rangle_{\Omega_J} = \langle \partial_{xj}(\mu(\partial_{xj}u_i + \partial_{xi}u_j)) \rangle_{\Omega_J}. \quad (2.2.8)$$

Assuming  $\vec{R}_J$  is constant within the control volume and application of the Gauss integration to the (Right Hand Side) RHS of equation 2.2.8 leads to the conditional equation for  $\vec{R}_J$ .

$$\vec{R}_J = \sum_m \langle \mu(\partial_{xj}u_i + \partial_{xi}u_j) \vec{n}_{Jm} \rangle_{\partial\Omega_{Jm}}. \quad (2.2.9)$$

Where  $\vec{n}_{Jm}$  is the outer normal vector of the surface  $\partial\Omega_{Jm}$ . Applying this formulation the fully resolved flow fields of the entire geometry must not be calculated. Nevertheless the  $\vec{R}_J$  for all coarse grid cells in their different thermodynamic states need to be calculated from the parametrized, representative segment data.

### Derivation of the Anisotropic Porosity Parameters

For the non-resolved geometrical information lacking in the coarse mesh, advantage is taken from an anisotropic porosity formulation that was originally implemented in the Commix code [3]. The anisotropic porosity formulation is based on the surface permeability  $\gamma_A$  the volume porosity  $\gamma_V$  and the distributed resistance. Within the formulation of the CGCFD the distributed resistance, which accounts for the friction between the submerged structure and the fluid, is represented by the volumetric source term  $\vec{R}_J$ . The porosity parameters are introduced into the Euler momentum equation.

$$\rho[\partial_t U_i + \gamma_A \partial_{xj}(U_i U_j)] + \gamma_V \partial_{xi} P = \vec{R}_J. \quad (2.2.10)$$

Volume- and surface averaging (2.3) of the convection term constrains the surface permeability for each control volume.

$$\langle \partial_{xj}(u_i u_j) \rangle_{\Omega_J} = \langle \gamma_A \partial_{xj}(U_i U_j) \rangle_{\Omega_J}. \quad (2.2.11)$$

Equation (2.11) applies Gauss integration and converts the volume integral into a surface integral across the surface  $\Omega_{Jm}$  of control volume J which is solved for the surface permeability  $\gamma_{AJm}$ .

$$\gamma_{AJm} = \langle u_i u_j \vec{n}_{Jm} \rangle_{\partial\Omega_{Jm}} \langle U_i U_j \vec{n}_{Jm} \rangle_{\partial\Omega_{Jm}}^{-1}. \quad (2.2.12)$$

Applying the same procedure to the pressure gradient the volume porosity  $\gamma_{VJ}$  is derived (2.13):

$$\langle \partial_{xi} p \rangle_{\Omega_J} = \langle \gamma_A \partial_{xi} P \rangle_{\Omega_J}, \quad (2.2.13)$$

$$\gamma_{VJ} = \langle \partial_{xi} p \rangle_{\partial\Omega_J} \langle \partial_{xi} P \rangle_{\partial\Omega_J}^{-1}. \quad (2.2.14)$$

The proposed Gaussian integration strategy represents a full closure.

The method is similar to the porous media approaches, although the porosity parameters are here geometrical derived and the viscous resistance factor as well as the inertial resistance factor is replaced by the volumetric source terms derived from the reference simulation.

### Treatment of the energy equation within the CGCFD

The energy equation for the CGCFD is implemented in the following manner:

$$\frac{\partial h}{\partial t} + \nabla \cdot (\vec{U}T) - \nabla \cdot \alpha_{coarse} \nabla T = \dot{q}, \quad (2.2.15)$$

with temperature T. Here the thermal conductivity  $\alpha_{coarse}$  is interpolated from the reference mesh to the coarse grid mesh. In case of a very coarse mesh the heat conductivity cannot be resolved so that the heat flux from the walls is replaced by a volume source term  $\dot{q}$ .





Our data basis for parameterization consists of four reference simulations employing k-Ω turbulence model and four Reynolds numbers as shown in Tab. II. The flow media is water with a kinematic viscosity  $\nu$  of  $8.93\text{e-}7 \text{ m}^2/\text{s}$ .

Polynomial interpolation of the volumetric source terms is carried out. Coefficients

$$a = (a(1), a(2), \dots, a(n)),$$

of the interpolation polynomial

$$p(x) = a_1x^n + a_2x^{n-1} + \dots + a_nx + P_{n+1},$$

are computed with a least square approach. This leads for the four reference simulations to a polynomial interpolation of the third degree for each individual cell of the coarse mesh. Figure 3-3 shows the fitting

**Table II. Conducted simulations for parameterization of volumetric source terms**

no.	no. cells	Re <sub>dHyd</sub>	y+
I	103680	20000	~22
II	151200	40000	~21
III	166320	60000	~21
IV	224640	80000	~20

function of the volumetric source term of a single coarse grid cell. Blue crosses within the figure are reference values of the RANS simulations used for the fit. The green dots are two additional reference simulations that are conducted but disregarded in the polynomial fit. Obviously fitting function (red) and these two simulations differ slightly. The additional simulations allow quantifying the error of CGCFD simulations conducted with parameterized volumetric forces outside of the parameterization range.

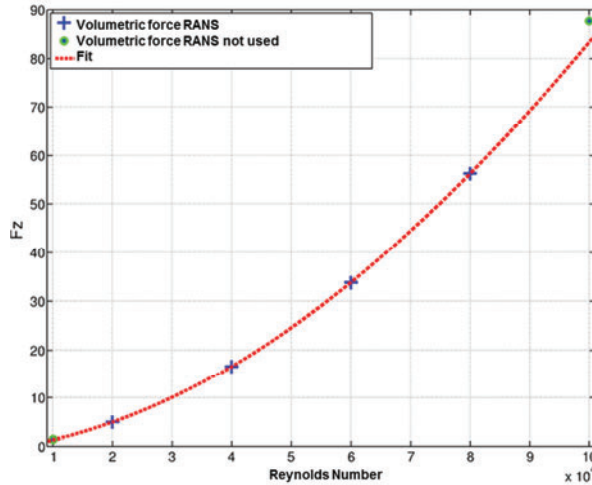
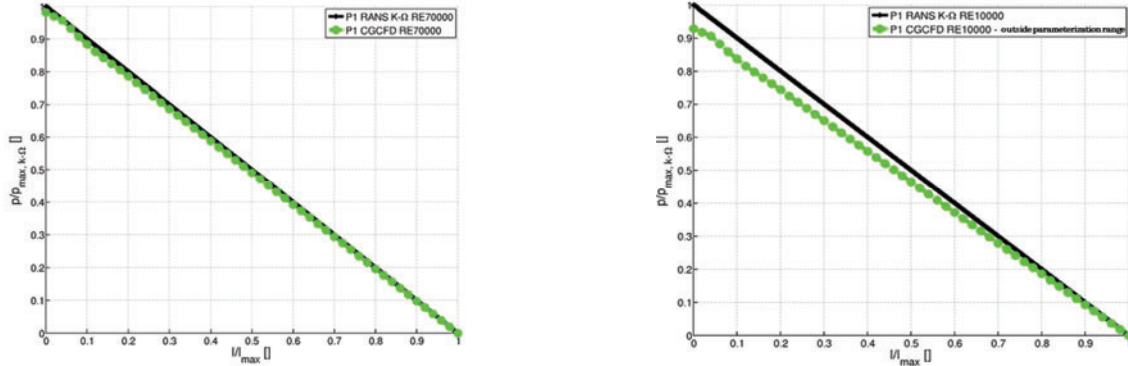


**Figure 3-3 Fitting function volumetric source terms. Blue crosses are reference values extracted from RANS CFD simulation and used for the fit. The green dots represent Reynolds numbers outside the parameterization range.**

CGCFD simulations employing parameterized volumetric force terms are conducted for Reynolds numbers of  $10^4$ ,  $3 \cdot 10^4$ ,  $5 \cdot 10^4$ ,  $7 \cdot 10^4$ ,  $10^5$  and  $1.2 \cdot 10^5$ . Evaluation of these simulations is realized by a comparison of the pressure profile of the CGCFD simulations respecting parameterized volumetric force terms to RANS CFD results. Figure 3-4 show two pressure profiles plotted along the subchannel. Figure 3-4 a) visualizes the pressure distribution of the CGCFD simulation respecting parameterized volumetric source terms (green), compared to the pressure distribution calculated with a RANS CFD simulation. The volumetric forces are within parameterization range and the Reynolds number for this simulation is  $7 \cdot 10^4$ . Figure 3.4 b) shows the same plot but now the CGCFD simulation is conducted with volumetric source terms outside of the parameterization range (green dots in Figure 3-3). The Reynolds number is  $10^4$ .

Table III summarizes the conducted simulations and their deviation compared to reference simulation at identical Re.



a) volumetric source term within parameterization range      b) volumetric source term outside of parameterization range

**Figure 3-4 Pressure distribution within subchannel: Comparison between CGCFD respecting parameterized volumetric source terms and reference simulation.**

**Table III. Conducted simulations for parameterization of volumetric source terms**

no.	no. cells	$Re_{dHyd}$	within parameterization range	$\frac{\Delta P_{RANS}}{\Delta P_{CGCFD}}$ in [%]
<i>I</i> <sub>CGCFD</sub>	2700	30000	Yes	97.95
<i>II</i> <sub>CGCFD</sub>	2700	50000	Yes	98.95
<i>III</i> <sub>CGCFD</sub>	2700	70000	Yes	98.3
<i>IV</i> <sub>CGCFD</sub>	2700	10000	No	95.01
<i>V</i> <sub>CGCFD</sub>	2700	100000	No	93.87
<i>VI</i> <sub>CGCFD</sub>	2700	120000	No	92.84

### Conclusion parameterization volumetric source terms

The conducted parameterization of the volumetric source terms demonstrates feasibility of an adequate parameterization. The used method is based on a simple parameterization approach, the polynomial interpolation. We propose to use more elaborate methodologies to perform such parameterizations such as parameterizations based on Proper Orthogonal Decomposition (PODs). Yet this paper already demonstrates feasibility of CGCFD employing parameterized volumetric source terms. In the demonstration case calculated pressure drop inside the subchannel deviates by no more than two percent as long as the simulations are performed within the parameterization range. This is a remarkably good result considering the simplicity of the parameterization method.

### 3.3. Validation of the implementation of the Energy equation for LBE cooled rod bundles

#### 3.3.1. Treatment of the energy equation for Lead Bismuth Eutectic (LBE) flows

Reference simulations for the thermal hydraulic investigation of the LBE cooled subchannel and rod bundle were conducted with temperature dependent quantities of LBE [5].

The reference RANS simulations used the energy equation in the form:

$$\frac{\partial T}{\partial t} + (\vec{u} \cdot \nabla)T - \alpha_{eff} \nabla^2 T = 0, \quad (3.3.1)$$

with effective thermal diffusivity  $\alpha_{eff}$ ,

$$\alpha_{eff} = \alpha_{lam} + \alpha_{turb}. \quad (3.3.2)$$

Laminar thermal diffusivity  $\alpha_{lam}$  can be calculated based on kinematic viscosity  $\nu$  and laminar Prandtl number,  $Pr_{lam,LBE} = 0.025$ .

$$Pr_{lam,LBE} = \frac{\nu}{\alpha_{lam}}. \quad (3.3.3)$$

Similarly, turbulent thermal diffusivity  $\alpha_{turb}$  can be calculated based on eddy viscosity  $\nu_t$  and turbulent Prandtl-number,  $Pr_{turb,LBE}$ .

$$Pr_{turb,LBE} = \frac{\nu_t}{\alpha_{turb}}. \quad (3.3.4)$$

Here turbulent Prandtl number is calculated employing the Kays correlation [6],

$$Pr_{turb,LBE} = \frac{0.7\alpha_{lam}}{\nu_t} + 0.85. \quad (3.3.5)$$

The Kays correlation estimates turbulent Prandtl number employing data of molecular thermal diffusivity and eddy viscosity.

To validate the implementation of the energy equation the reference simulation was compared to a LES simulation conducted in [4]. Figure 3-5 shows the dimensionless temperature  $T^+$  non-dimensionalized with the wall shear stress temperature based on the wall friction velocity  $u_\tau$ :

$$T_\tau = \frac{\alpha_{lam}}{u_\tau} \left. \frac{\partial T}{\partial y} \right|_{wall}. \quad (3.3.6)$$

Red dots in the figure represent the LES simulation and the black line shows results of the RANS CFD simulation. The temperature in the free stream is underestimated by the RANS CFD simulation. Nevertheless the results show that RANS simulation predicts temperature profiles with an acceptable agreement.

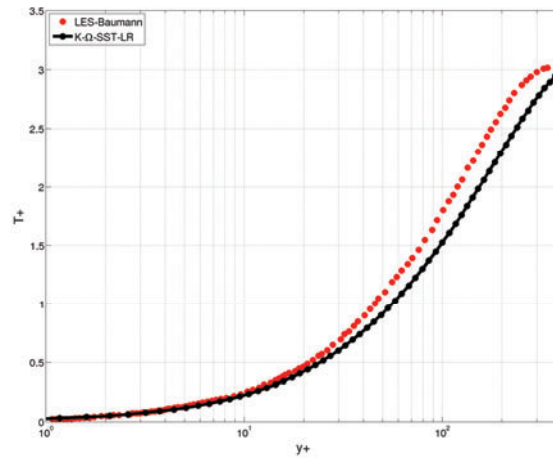


**Figure 3-5. Dimensionless temperature profile of reference simulation compared to a LES simulation.**

### 3.3.2. Energy equation treatment within the CGCFD

For the CGCFD method two approaches of treating the energy equation are proposed. The best choice between these approaches depends on the resolution of the coarse mesh. The first approach (I) neglects the diffusive energy transport:

$$\frac{\partial T}{\partial t} + (\vec{u} \cdot \nabla)T = \dot{q}. \quad (3.3.7)$$

A heat source is directly entered into all coarse cells.

The second approach (II) respects diffusive energy transport:

$$\frac{\partial T}{\partial t} + (\vec{u} \cdot \nabla)T - \alpha_{coarse} \nabla^2 T = \dot{q}. \quad (3.3.8)$$

Thermal diffusivity  $\alpha_{\text{coarse}}$  is interpolated from the reference simulation to the coarse mesh. This approach of course needs a higher coarse mesh resolution than approach I. Figure 3-7 shows typical mesh resolutions of a subchannel for approach I (Figure 3-6 a) and approach II (Figure 3-6 b)).



a) CGCFD Mesh resolution approach I)

b) CGCFD Mesh resolution approach II)

**Figure 3-6. Mesh resolutions for CGCFD simulation.**

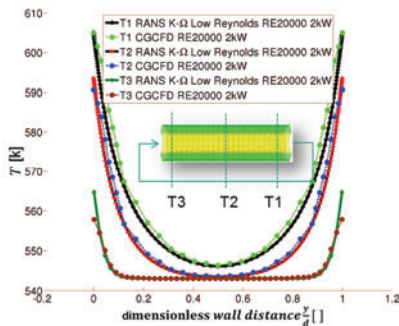
Table IV summarizes numerical settings as well as results from the simulation with approach (I). In the simulation the heat source was directly entered into the coarse mesh cells. The very coarse resolution forbids resolving cross-sectional temperature. To quantify results the averaged outlet temperature of the CGCFD simulation of the subchannel is compared to averaged outlet temperature of the reference RANS CFD simulation (Compare Table IV).

Note that this approach is suitable for system wide simulations e.g. a complete reactor core, where subchannels are resolved via a few cells only. Along the height of a subchannel/ fuel assembly the heating power profile is be considered by an appropriate heat source similar to subchannel analysis. More information about this approach can be found in [7].

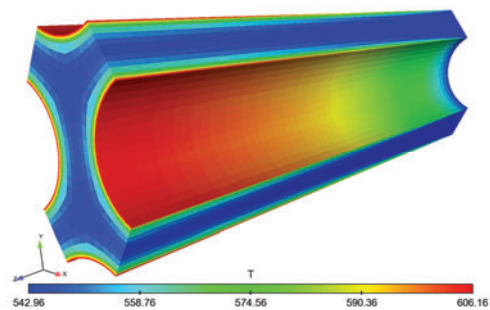
The second approach interpolates thermal diffusivity from the reference simulation to the CGCFD simulation. With this approach it becomes possible to resolve the cross-sectional temperature profile. Figure 3-7 shows results of the CGCFD simulation of the subchannel with approach (II). In figure 3-7 a) the temperature is plotted at three different positions inside the rod bundle. The positions are marked within the subfigure. Figure 3-7 b) shows temperature distribution within the complete subchannel. The used CGCFD mesh has 23040 computational cells, which represents significant reduction compared to the reference simulation.

**Table IV. Conducted simulations for parameterization of volumetric source terms**

no.	no. Cells	turb. model	heating rate	averaged outlet temp approach (I) 1KW
<b>RANS</b>	1.3 Million	k- $\Omega$ -SST-LR	0.5/1/2 KW	578.608 K
<b>I<sub>CGCFD</sub></b>	3500	CGCFD	0.5/1/2 KW	579.308 K
<b>II<sub>CGCFD</sub></b>	23040	CGCFD	0.5/1/2 KW	578.407K



a) temperature profile subchannel



b) temperature distribution within subchannel

**Figure 3-7 Temperature distribution CGCFD simulation in comparison with reference Simulation.**

### Conclusion Energy equation treatment within the CGCFD

The CGCFD method is capable to resolve temperature profiles if approach (ii) and an adequate mesh resolution is chosen. On yet coarser meshes approach (I) still allows computing averaged subchannel temperatures. The method allows exploring the effect of distinct individual heating rates of individual rods.

## 4. APPLICATION OF THE CGCFD METHOD TO FUEL ASSEMBLIES

### 4.1. CGCFD simulation of a LBE cooled 19 pin fuel rod bundle with wire wrapped spacer grids.

The 19 pin fuel rod bundle is investigated experimentally at the KALLA laboratory at the KIT. The reference simulation for the CGCFD simulation is conducted with the  $k-\Omega$ -SST turbulence model and includes one wire pitch. More information about the detailed simulation can be found in [8]. For the CGCFD simulation a computational grid with 92000 cells is used. Figure 4-1 shows both domains the RANS CFD computational domain as well as the CGCFD domain. Due to the coarse mesh the wires are not geometrical resolved, instead they are resolved by the anisotropic porosity formulation that is explained in detail in [2]. The boundary conditions for the CGCFD simulation can be found in Table V and Figure 4-1. The volumetric source terms needed for the CGCFD simulation were extracted from the 19 pin RANS reference simulation and interpolated within the CGCFD mesh. Figure 4-2 shows a comparison of the velocity profile within a cross section of the rod bundle and the corresponding pressure drop. Figure 4-2 a) represents the RANS simulations whereas figure 4-2 b) shows the CGCFD results. The main flow features are captured by the CGCFD simulation. The velocity at the boundary of the bundle is accelerated due to the wires. This effect is captured by the CGCFD simulation. Also the anisotropic porosity formulation is able to reduce the velocity at the positions of the wire. Figure 4-2 c) shows the dimensionless pressure drop non-dimensionalized by the maximum pressure of the reference CFD simulation. The pressure profile is in good agreement compared to the reference simulation. The measurement position is marked in the figure.

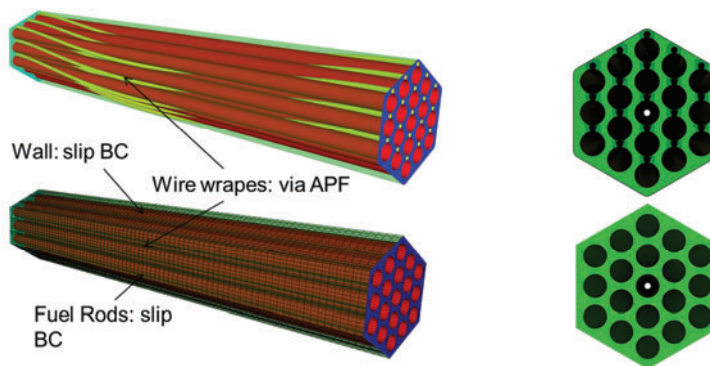
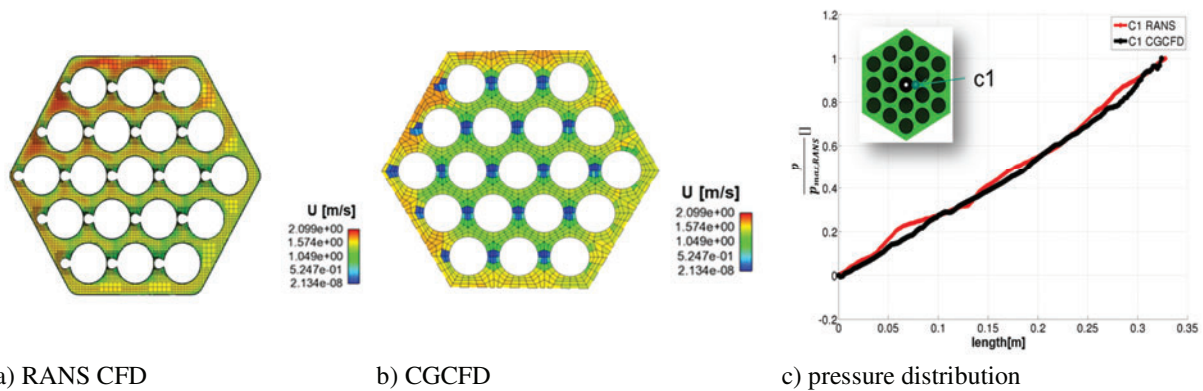


Figure 4-1. Computational domain with boundary conditions for CGCFD simulation.

Table V. Conducted simulations for parameterization of volumetric source terms

no.	no. cells	turb. model	$U_{Inlet}$	mesh reduction factor
RANS	13.5 million	k- $\Omega$ -SST	1.5 m/s	-
CGCFD	92000	CGCFD	1.5 m/s	147



**Figure 4-2. Comparison between RANS CFD and CGCFD simulation**

#### 4.2. Conclusion CGCFD simulation of a LBE cooled 19 pin fuel rod bundle with wire wrapped spacer grids.

The results of the CGCFD simulation show good agreement to the detailed reference simulations. The pressure distribution as well as the velocity profile is captured by the CGCFD. The global velocity distribution of the detailed CFD simulation as well as details around the wire wraps are captured by the CGCFD method.

#### 4.3. CGCFD simulation of a LBE cooled 127 pin fuel rod bundle with wire wrapped spacer grids.

To demonstrate feasibility of a large CGCFD a 127 pin fuel bundle simulation is conducted. The previous 19 pin fuel rod bundle is exploited as reference simulation. Using such a large reference simulation is normally not suggested but since it was available it was explored. The smallest possible reference geometry would require generating a mesh with perfectly collocated control volumes, taking into account wire wraps. Mesh generation would exceed the total computational time and effort. Therefore the volumetric forces, as well as the surface permeability and the volume porosity were interpolated from the smaller 19 pin fuel rod simulation to the 127 pin bundle according to their position.

The effect that leads to smaller pressure drops as well as lower velocities, if a smaller bundle is compared to a larger with the same boundary conditions, is not fully accounted for with this interpolation. Therefore the correlation of Cheng-Todreas [9] was used to calculate an adjustment factor for the volumetric source terms. The friction pressure drop is calculated as follow:

$$\Delta p = f \frac{L}{A 2 D_{Hyd}} \rho v^2, \quad (4.3.1)$$

with the pressure drop in Pascal  $\Delta p$ , the friction factor  $f$ , the length in meter  $L$ , the hydraulic diameter  $D_{Hyd}$ , the fluid density  $\rho$  and the axial velocity  $v$ . The Cheng-Todreas correlation is used to evaluate the friction factor. Two formulations of the correlation are valid. Here the simplified form for a turbulent flow regime and consideration of the whole bundle is described:

$$c_{ft} = \left[ 0.8063 - 0.9022 \cdot \log\left(\frac{H}{D}\right) + 0.3526 \cdot \log\left(\frac{H}{D}\right)^2 \right] \cdot \left(\frac{P}{D}\right)^{9.7} \cdot \left(\frac{H}{D}\right)^{1.78-2*\left(\frac{P}{D}\right)}, \quad (4.3.2)$$

with pin pitch  $P$ , pin diameter  $D$  and wire pitch  $H$ . The friction factor for a turbulent regime is:

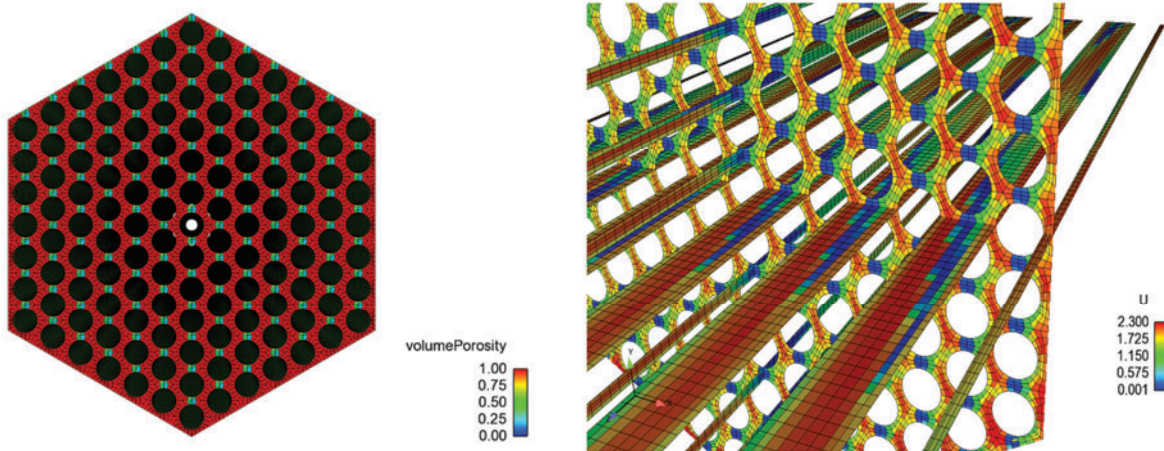
$$ft = \frac{C_{ft}}{Re^{0.18}}, \quad (4.3.3)$$

with bundle averaged Reynolds number  $Re$ . Table VI shows the Cheng-Todreas estimated pressure drop compared to the 19 pin reference case. Also the calculated CGCFD pressure drop is compared to the 19 pin RANS CFD reference simulation as shown in the table.

Figure 4.4 a) shows the cross section of the fuel bundle with the volume porosity that represents non-resolved wires. Figure 4.4 b) shows the velocity distribution inside the rod bundle.

**Table VI. Pressure drop of fuel bundles with different number of rods compared to pressure drop of the 19 pin rod bundle**

Number of Pins	$\left(\frac{dp}{dz}\right) * \left(\frac{dp_{19}}{dz}\right)^{-1} \text{C\&T}$	No. Cells CGCFD	$\left(\frac{dp_{19}}{dz}\right) * \left(\frac{dp_{CGCFD}}{dz}\right)^{-1} \text{CGCFD}$
19	1	92000	0.987
37	0.9850	-	-
61	0.9735	-	-
91	0.9648	-	-
127	0.9581	1075200	0.946



a) CGCFD mesh with volume porosities representing the wire wraps.

b) velocity profile 127 pin bundle

**Figure 4-4. CGCFD Mesh and velocity profile inside the bundle.**

#### 4.4. Conclusion CGCFD simulation of a LBE cooled 127 pin fuel rod bundle with wire wrapped spacer grids.

The CGCFD simulation of the 127 pin bundle demonstrates that the method is applicable when simulating large domains. More validation work is work in progress, and in particular the use of the Cheng-Todreas correlation will be omitted in the future. Nevertheless the CGCFD simulation showed that it is possible to perform such, under normal conditions extremely time and money consuming simulations, in a fast and computational effective way. Of course a sound validation of this simulation has to be performed. This could be done by either a RANS or LES simulation like [13] has demonstrated. At this stage of the development of the method this simulation is primarily carried out to show the possibilities of the methodology.

## 5. CONCLUSIONS

The CGCFD method, is under development at the AREVA Nuclear Professional School (ANPS) of the Karlsruhe Institute of Technology (KIT). The CGCFD method uses detailed CFD simulations of components of a complete system that is under investigation to extract volumetric forces parametrized in an appropriate way. The parametrized volumetric forces then enter the CGCFD governing equations as source terms, replacing non resolved physical effects due to the use of an Euler solver and very coarse

meshes, resolving the subchannel scale. With this method a 3D simulation of the complex system is possible in a computational- and cost effective way. The methodology is first applied to a straight sub channel test case evolving to quiet complex cases, e.g. the simulation of a wire wrapped fuel assembly. The simulation of the sub channel and the described parametrization of the volumetric forces demonstrate how a CGCFD simulation of a complete reactor core could be performed in future. The parametrized CGCFD results are in good agreement with the corresponding detailed CFD simulations, even though more sophisticated parametrization strategies are proposed. Therefore in future evolutions of the method a focus should lay on development and implementation of more advanced parametrization methods. These could rely on Proper Orthogonal Decomposition of the volumetric source terms. Certainly, the CGCFD method requires educated user input to identify the representative patterns of the geometry. Then volumetric forces can be extracted from detailed simulations which are much smaller than the original target of investigation. Detailed CFD simulations, e.g. RANS or LES, need to follow CFD best practice guidelines or proper verification and validation. By well-chosen parametrization the detailed CFD database can be substantially reduced which represent a current research topic. Since the flow in considered applications has repetitive character, the costs of representative CFD simulations employed to extract volumetric forces is much lower than a full simulation. Coarse meshes and less complex equations allow using this method to compute a full reactor core and the adjacent plena in a single cost-effective CFD simulation. In contrast to a sub channel analysis some details below the sub channel scale are retained thus providing insight into local phenomena.

## REFERENCES

1. A. Batta, A. Class, K. Litfin T. Wetzel, "Numerical Study on Flow Distribution and Turbulent Flow in XT-ADS Rod Bundle Water Experiment," *NUTHOS-8 Shanghai 2010*.
2. M. Viellieber, A. Class, "Anisotropic Porosity Formulation of the Coarse-Grid-CFD (CGCFD)", Proceedings of the 2012 20<sup>th</sup> International Conference on Nuclear Engineering, ICONE20, Anaheim.
3. T. H. Chien, H. M. Domanus, and W. T. Sha, "COMMIX-PPC: A Three-Dimensional Transient Multicomponent Computer Program for Analyzing Performance of Power Plant Condensers", ARGONNE NATIONAL LABORATORY
4. T. Baumann, "Turbulenzmodellierung von Strömungen niedriger molekularer Prandtlzahl," *Doctoral Thesis*, Karlsruhe Institute of Technology, (2012).
5. *Handbook on Lead-bismuth Eutectic Alloy and Lead Properties, Materials Compatibility, Thermal-hydraulics and Technologies*, NUCLEAR ENERGY AGENCY (2007).
6. M. Kays, "Turbulent Prandtl Number-Where Are We?," *ASME* , pp. 284-295 (1994).
7. S. Himmel, "Modellierung des Strömungsverhaltens in einem HPLWR-Brennelement mit Drahtwendelabstandshaltern," *Doctoral Thesis*, Karlsruhe Institute of Technology, (2009).
8. M. Raquet, „CFD Analyse lokaler Versperrungen in Stabbündeln“ *Master Thesis*, Karlsruhe Institute of Technology, (2014).
9. Shih-Kuei Cheng and Neil Todreas, "Hydrodynamic Models and Correlations for Bare- Wire-Wrapped-Hexagonal Rod Bundles- Bundle Friction Factors, Nuclear Engineering and Design, 1986
10. P. Dietrich, Coarse-Grid-CFD (CGCFD) eines Brennstabbündels mit Drahtwendelabstandshaltern, *Master Thesis*, Karlsruhe Institute of Technology, (2013).
11. Roelofs, F., Gopala, V., Chandra, L., Viellieber, M., & Class, A. Simulating fuel assemblies with low resolution CFD approaches *Nuclear Engineering and Design*, S. 548-559.
12. Viellieber, M., Dietrich, P., & Class, A. (10 2013). Investigation of a Wire Wrapped Fuel Assembly with the Anisotropic Coarse-Grid-CFD. *International Journal for Nuclear Power*, S. 573-575.
13. Pointer , D. W., Thomas , J., Fanning, T., Fischer, P., Siegel, A., Smith, J., et al. (2009). RANS BASED CFD SIMULATIONS OF SODIUM FAST REACTOR WIRE-WRAPPED PIN BUNDLES. *International Conference on Mathematics, Computational Methods & Reactor Physics*.